Supporting information

D. Bratko[1,2,a,*], C. D. Daub[1], K. Leung[3] and A. Luzar[1,b,*]

[1]Department of Chemistry, Virginia Commonwealth University, Richmond, VA 23284-2006

[2]Department of Chemical Engineering, University of California, Berkeley, CA 94720-1462

[3]Sandia National Laboratories, MS 1421, Albuquerque, NM 87185

a: dnb@berkeley.edu, b: aluzar@vcu.edu

S.I Macroscopic relations

Electrowetting on macroscopic surfaces is usually characterized in terms of contact angle, $0<\theta_c,<180^o$, defined by Young equation $\cos\theta_c=(\gamma_{sv}-\gamma_{sl})/\gamma_{lv}$, where γ_{ab} is the surface free energy between solid (s), liquid (l) and vapor (v) phases. A change from negative to positive $\cos\theta_c$ implies a transition from drying to wetting behavior, hence we refer to surfaces with $\theta_c>90^o$ as hydrophobic and those with $\theta_c<90^o$, hydrophilic.

Electrocapillarity in a planar confinement can be described by an equation of the form:

$$\cos\theta_c = \frac{\gamma_{sv}-\gamma_{sl}}{\gamma_{lv}} - \frac{W_{el}(V)}{2\gamma_{lv}} = \cos\theta_c^o - \frac{W_{el}(V)}{2\gamma_{lv}} \qquad \text{(S.1)}$$

Here $W_{el}(V)$ is the change in electrostatic energy per unit area, associated with surface spreading of the liquid, wetting both walls (hence the factor 1/2), V is the voltage across the interface, and θ_c^o is the contact angle in the absence of electric field. The form of W_{el} depends on system geometry and material properties but is generally presumed to be proportional to the areal electric capacitance of the interface, c, and the potential drop across the interface squared, $W_{el} \sim -\frac{c}{2}V^2$ [1,2].

We consider electrocapillarity in water-filled planar nanopores in a uniform external field E_o. Notwithstanding its weak ionization, water in a *nanopore* behaves as a dielectric of relative permittivity ε_r because the double layer screening length associated with water ions exceeds the pore width by at least two orders of magnitude. The field E_o can arise due to opposite charges on the plates of a capacitor[3] or can be attributed to locally unbalanced charges in the environment. The confinement is open to exchange of water with field-free reservoir at ambient

temperature and pressure and is fully described by specifying the values of chemical potential μ, volume AD ($A>>D^2$ is the plate area and D inter-plate separation), temperature T, and field strength E.

For a uniform field, the difference between electrical energies of water-filled (l) and empty (e) pores, treated as capacitors with areal capacitances $c_e=\varepsilon_0/D$ and $c_l=\varepsilon_r\varepsilon_0/D$, gives[4]:

$$W_{el} = W_l - W_e = \frac{D}{2}(\varepsilon_r\varepsilon_0 E^2 - \varepsilon_0 E_0^2) \approx -\frac{\varepsilon_0 D}{2}E_0^2 \qquad \text{(S.2)}$$

In the above, $E_0=V_0/D$ is the applied electric field across the slit before reduction due to water polarization ($E_o \to E \approx E_o/\varepsilon_r$). Eqs S.1 and S.2 suggest an expression for apparent contact angle $\cos\theta_c=\cos\theta_c^o+\varepsilon_o DE^2/4\gamma_{lv}$. Note that W_{el} is associated with volume rather than with the surface layer alone.

In addition to increased surface wettability, favorable interaction of polar liquid with electric field results in increased liquid density ρ. To the first order, electrostriction is given by

$$d\ln\rho \approx \frac{\kappa\rho\varepsilon_o}{8\pi}\frac{\partial\varepsilon_r}{\partial\rho}d(E^2), \qquad \text{(S.3)}$$

where κ is isothermal compressibility[5]. In common with predictions for other geometries, in weak fields eqs S.2-3 imply that the change in contact angle and relative increase in local density of the liquid vary in proportion to field squared. Eq S.1, combined with an appropriate estimate of areal capacitance of the surface, provides the basis for techniques involving electrically tunable hydrophobic/hydrophilic surfaces[2,6,7] while eq S.2 offers a qualitative explanation of the role of ions in gating of biological channels[8,9].

In narrow hydrophobic confinements, unfavorable surface energetics can trigger spontaneous liquid-to-vapor transition termed capillary evaporation. The thermodynamic condition for evaporation from between extended planar surfaces is given by Kelvin equation[10], which can be written[11,12] in the form $D \le D_c^o=2(\gamma_{sl}-\gamma_{sv})/P$ where P is the pressure. Generalization to systems in a weak electric field E_o has shown that the field reduces the evaporation threshold width to $D_c(E) \sim D_c^o P/(P+\frac{\varepsilon_0 E_0^2}{2})$ [4].

For stronger fields E above ~ O(10^{-2}) V $\mathring{A}^{-1}$, corresponding to nonscreened field E_o O(10^{-1}) V $\mathring{A}^{-1}$ deviations from quadratic dependencies on field strength are expected because of dielectric saturation. Further, by ignoring the molecular structure of the medium, including orientational preferences of surface molecules[13,14], continuum approximations should become inaccurate in nano-scale systems where the fraction of molecules in the boundary layer of the liquid is significant[3]. As shown in the main text, our simulations in nano-sized systems confirm qualitative trends predicted by continuum models but reveal considerable quantitative deviations and demonstrate a strong dependence of surface wetting on field *direction* and *polarity*, a new behavior at variance with observations in and theories applicable to macroscopic systems.

S.II Interaction potentials

Interaction between water molecules and the confinement walls is described by integrated (9-3) Lennard Jones potential[11,13,15]

$$u_w(z) = A\left(\frac{\sigma_{C_hw}}{D' \pm z}\right)^9 - B\left(\frac{\sigma_{C_hw}}{D' \pm z}\right)^3 \qquad \text{(S.4)}$$

Here, $A = 4\pi\rho_{C_h}\varepsilon_{C_hw}\sigma^3_{C_hw}$ /45 and B=15A/2, D'=D/2, z is the distance of water oxygen from the slit midplane with walls at $z=\pm D'$, ρ_{Ch} is the number density of hydrocarbon CH_n groups, ε_{Chw} and σ_{Chw} are Lennard-Jones potential depth and size parameters for water oxygen-hydrocarbon CH_n group pair, and the sign $\pm$ in the denominators means we use opposite signs for interactions with the two walls. ε_{Chw} and σ_{Chw} are Berthelot's means for water oxygen and CH_n group Lennard-Jones parameters given in Table S.I. According to the above definitions, the slit

Table S.I. Lennard-Jones potential parameters describing the interaction of different atomic species, α(oxygen and hydrogen atoms in water (w) and CH_n groups in hydrocarbon (*h*).

α	ε_α/J mol^{-1}	q_α/e_o	$\sigma_\alpha/\mathring{A}$
O_w	650.2	-0.8476	3.1656
H_w	0.00	0.4238	-
CH_n	553.1	0.0	3.754

width actually occupied by water molecules will be close to D-σ_{Chw}.

Recent comparisons[16] between different interaction-site simulation models of water showthat calculated surface tensions of water are relatively robust with respect to details of model potential. The presence of external field may suggest the use of polarizable models, however, even for the non-screened fields E_o, the strengths we consider are weak compared to molecular and ionic fields that lead to visible polarization of a water molecule. According to fig. 6 of ref.[17], for fluctuating-charge (TIP4P-FQ)[18] polarizable force field of water, the strongest field considered in the present study, E=0.4 1V $\mathring{A}^{-1}$, will produce about 1% change in the average dipole moment of a water molecule.

S.III Pressure tensor calculation

Average pressure tensor components $P_\perp \equiv P_{zz}$ and $P_\parallel \equiv P_{xx} = P_{yy}$ were calculated from energy differences ΔU_α associated with uniform scaling of molecular coordinates α (α=z or x,y) and volume change ΔV_α. Here, ΔU_α comprises changes in intermolecular and water-wall interactions. Scaling of molecular center-of-mass positions, on the other hand, has no effect on interactions with the applied electric field. When lattice sums were applied in total energy calculations, proper care was taken to avoid double counting of replica/central box interactions in calculating the energy change ΔU_α upon coordinate scaling:

$$P_{\alpha\alpha} = \rho kT + lim_{\Delta V_\alpha \to 0} \frac{kT\, ln < exp(-\frac{\Delta U_\alpha}{kT}) >}{\Delta V_\alpha} \qquad \text{(S.5)}$$

Forward and backward scaling was employed for improved accuracy. A coordinate- scaling factor f=$1 \pm \delta$ with δ=10^{-5} was chosen empirically for optimal compromise between round-off errors (decreasing with increasing δ) and the numerical accuracy of the finite difference approximation employed in eq S.4 (improved upon decreasing δ). Variation of δ within the interval $10^{-6} \leq \delta \leq 10^{-4}$ revealed no appreciable effect on calculated pressure components. The calculated normal component of the pressure tensor, $P_{zz} \equiv P_\perp$, was found to agree within numerical uncertainty with wall pressure calculated directly from wall/water forces as described in our earlier work[11].

S.IV Energy reduction in electric field

Figs. S.1 and S.2 illustrate the field-dependence of average reduced molecular energy, U/NkT, for bulk water, a water slab with free liquid/vapor surfaces (slab thickness of approximately seven molecular diameters, unlimited in lateral directions), and confined water in paraffin-like pores of width D=1.64 or 2.7 nm. For inhomogeneous systems, directions of the field perpendicular and parallel to water layer surfaces were considered. Polarization energy correction[19] for SPC/E model was not included in reported energies.

In Fig. S.1 we present results for bulk (triangles) and interfacial (squares) water in contact with the vapor phase. The average difference between bulk water and interfacial water in ~ seven layer slab of water, $(U_{slab}-U_{bulk})/NkT$=0.79 kT translates to surface energy of 112 mN/m, very close to the experimental value of 117 mN/m [20,21]. In all cases we observe approximately quadratic energy decrease with the field strength. Interestingly, in the perpendicular field, the difference between the energies of interfacial water and water in the bulk phase depends only weakly on field strength. This is explained in terms of canceling effects of molecular alignment on the two opposite walls. On one wall, the two hydrogens are more likely to point into the liquid phase, an orientation relatively favorable for hydrogen bonding. On the opposite wall, the field tends to orient surface molecules with hydrogens pointing toward the wall, reducing opportunities for hydrogen bonding. In the parallel field, however, as the field gets stronger, the parallel alignment of surface molecules supports hydrogen bonding and the difference between interfacial and bulk water diminishes with increasing strength of the field. Overall, however, the effect of field *direction* on water at the liquid/vapor interface is weaker than for confined water (Fig S.*2*).

Confined water, illustrated in Fig. S.2, features a qualitatively similar dependence on the applied field, however, the effect of field direction, producing lower energies in parallel field, is more pronounced. This is particularly true for the narrower confinement, confirming that the difference comes from surface molecules, whose fraction is higher in narrower slits. Since water polarization is strongest at the surface[22], accumulation of water molecules in surface layers optimizes favorable interactions with the field. In stronger fields, alignment of water dipoles is inadvertently accompanied by some reduction of hydrogen bonding. This loss is partly compensated by increased attractive interaction between oxygen atoms and the wall,

accompanying the buildup of interfacial liquid can acquire lower energy than the bulk fluid at equal field strength.

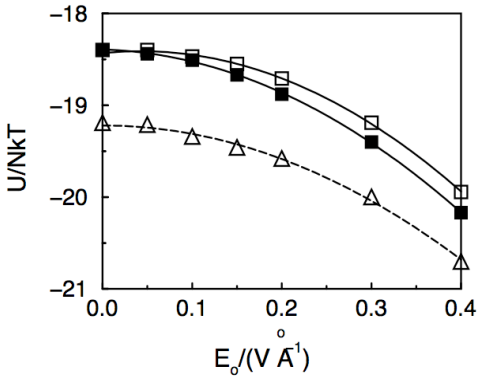

Figure S.1 Average configurational energy per water molecule, $\langle U \rangle / NkT$, as a function of the strength of applied field, E_o, in bulk aqueous phase (triangles), or within a semi-infinite aqueous slab of width corresponding to approximately seven molecular layers (squares) for perpendicular (empty) or parallel (filled symbols) direction of the field.

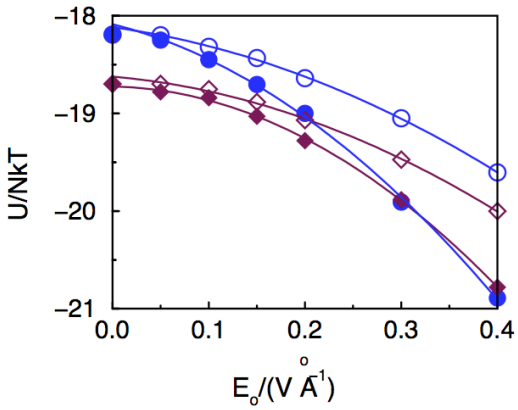

Figure S.2 Average configurational energy per water molecule, $\langle U \rangle / NkT$, as a function of the strength of applied field, E_o, in a hydrocarbon-like confinement of width 1.64 nm (blue) or 2.7 nm (magenta) for perpendicular (empty) or parallel direction (solid symbols) of the field.

S.V Surface tensions in field-free systems

For proper characterization, in Table S.II we first list our results for surface tension of pure water (determined for semi-infinite liquid slab in contact with vapor), γ_{lv}, and surface free energies σ, pertaining to wetting of hydrocarbon-like confinement walls, as defined in eq 1 in the main text, for planar hydrocarbon confinement of width 2.7 nm. Periodic boundary conditions were used in lateral directions *x,y*. In most cases, lateral box size L_{xy} was 2.1 nm, twice the cutoff radius of 1.05 nm, and 1.8 nm in the few cases employing 0.85 nm cutoff. While listed σ values correspond to a finite confinement width, we notice no appreciable dependence of σ on *D*, hence the results in field-free systems can be

Table S.II. Interfacial free energies for a water slab of thickness of about seven molecular layers in contact with vapor, γ_{lv}, and in hydrocarbon-like confinement of width *D*=2.7 nm, $\sigma \sim (\gamma_{sl}-\gamma_{sv})$ for SPC and SPC/E potentials of water, and effective contact angle $\theta_c \sim -\cos^{-1}(\sigma/\gamma_{lv})$.

	Spherical cutoff	γ_{lv} / mN m^{-1}	σ/ mN m^{-1}	θ_c
SPC/E	1.05 nm	50 ± 3	36.5 ± 3	137 ± 5^o
SPC/E	0.85 nm	51 ± 3	37.6 ± 2	138 ± 5^o
SPC/E	none, 2-D Ewald	57 ± 4	36 ± 5	129 ± 10^o
SPC	0.85 nm	43 ± 2	31.3 ± 2	136.5 ± 6^o

regarded as close estimates of $\Delta\gamma=\gamma_{sl}-\gamma_{sv}$ for isolated or widely separated surfaces. To establish connection with previous works, where we used SPC water potential and identical water/wall interactions[11,15], in addition to SPC/E value obtained with current cutoff distance of 1.05 nm, we include results for both SPC and SPC/E models determined using the smooth water-water potential cutoff[14] of 0.85 nm. We also include the result for surface tension of aqueous slab obtained for SPC/E model using two- dimensional lattice sums. Prohibitive computation costs precluded the use of the combination of the MMM2D lattice sum routine in combination with the Grand Canonical algorithm necessary for confinement simulations. It is interesting to note the

comparatively weak dependence of calculated surface tensions and contact angle on the magnitude of the potential cutoff in present examples. In another study of the influence of spherical cutoff radius, Jaffe and coworkers observed[23] a considerably stronger dependence of contact angles for water on graphite, where cutoff range of about 1.5 nm was required to secure convergence. However, unlike our present work, in their calculations the cutoff was also applied to water-wall interactions explaining the stronger cutoff effect in their model.

Our result for the surface tension of the water slab of finite width, γ_{lv}~(57 ± 3) mN m^{-1}, obtained using two-dimensional lattice summation is lower than some literature estimates[24,25]. The difference can be attributed to the smaller thickness of the slab, however, a similar estimate, γ_{lv}~55 mN m^{-1}, has recently been obtained for *bulk* SPC/E water by two independent methods, from pressure tensor calculations[16], and from simulated capillary wavelength amplitudes[16]. According to our results, omission of lattice sums results in about 14% reduction in calculated surface tensions. Interestingly, switching from the SPC/E to SPC water potential has almost no effect on the calculated contact angle, following compensation of simultaneous decreases in liquid/vapor and solid/liquid terms. We also note that the surface tension for SPC water obtained from the difference of normal and tangential pressure components agrees with direct calculation of contact angle of confined water, θ_c=135$^o \pm 5^o$, described in earlier work[15].

References:

(1) Shapiro, B.; Moon, H.; Garrell, R. L.; Kim, C. J. *Journal Of Applied Physics* **2003**, *93*, 5794.

(2) Mugele, F.; Baret, J. C. *Journal Of Physics-Condensed Matter* **2005**, *17*, R705.

(3) Bateni, A.; Laughton, S.; Tavana, H.; Susnar, S. S.; Amirfazli, A.; Neumann, A. W. *Journal Of Colloid And Interface Science* **2005**, *283*, 215.

(4) Dzubiella, J.; Hansen, J. P. *Journal Of Chemical Physics* **2004**, *121*, 5514.

(5) Vaitheeswaran, S.; Yin, H.; Rasaiah, J. C. *Journal Of Physical Chemistry B* **2005**, *109*, 6629.

(6) Mugele, F.; Klingner, A.; Buehrle, J.; Steinhauser, D.; Herminghaus, S. *Journal Of Physics-Condensed Matter* **2005**, *17*, S559.

(7) Krupenkin, T.; Taylor, J. A.; Kolodner, P.; Hodes, M. *Bell Labs Technical Journal* **2005**, *10*, 161.

(8) Dzubiella, J.; Allen, R. J.; Hansen, J. P. *Journal Of Chemical Physics* **2004**, *120*, 5001.

(9) Vaitheeswaran, S.; Rasaiah, J. C.; Hummer, G. *Journal Of Chemical Physics* **2004**, *121*, 7955.

(10) Evans, R.; Parry, A. O. *Journal Of Physics-Condensed Matter* **1990**, *2*, SA15.

(11) Bratko, D.; Curtis, R. A.; Blanch, H. W.; Prausnitz, J. M. *Journal Of Chemical Physics* **2001**, *115*, 3873.
(12) Lum, K.; Luzar, A. *Physical Review E* **1997**, *56*, R6283.
(13) Lee, C. Y.; McCammon, J. A.; Rossky, P. J. *Journal Of Chemical Physics* **1984**, *80*, 4448.
(14) Shelley, J. C.; Patey, G. N. *Molecular Physics* **1996**, *88*, 385.
(15) Leung, K.; Luzar, A.; Bratko, D. *Physical Review Letters* **2003**, *90*, 065502.
(16) Ismail, A. E.; Grest, G. S.; Stevens, M. J. *Journal of Chemical Physics, in press*. **2006**.
(17) Yang, K. L.; Yiacoumi, S.; Tsouris, C. *Journal Of Chemical Physics* **2002**, *117*, 337.
(18) Rick, S. W.; Stuart, S. J.; Berne, B. J. *Journal Of Chemical Physics* **1994**, *101*, 6141.
(19) Berendsen, H. J. C.; Grigera, J. R.; Straatsma, T. P. *Journal Of Physical Chemistry* **1987**, *91*, 6269.
(20) Riddick, J. A.; Burger, W. B. *Techniques of chemistry*; Wiley-Interscience: New York, 1970; Vol. 2.
(21) Weast, R. C. E. *Handbook of chemistry and physics*; CRC: Cleveland, 1979.
(22) Ballenegger, V.; Hansen, J. P. *Journal Of Chemical Physics* **2005**, *122*.
(23) Jaffe, R. L.; Gonnet, P.; Werder, T.; Walther, J. H.; Koumoutsakos, P. *Molecular Simulation* **2004**, *30*, 205.
(24) Shi, B.; Sinha, S.; Dhir, V. K. *Journal of Chemical Physics, in press*. **2006**.
(25) Alejandre, J.; Tildesley, D. J.; Chapela, G. A. *Journal Of Chemical Physics* **1995**, *102*, 4574.